Autofocusing imaging: Imaging with primaries, internal multiples and free-surface multiples

Satyan Singh[1], Roel Snieder[1], Jyoti Behura[1,3], Joost van Der Neut[2], Kees Wapenaar[2], and Evert Slob[2]

(1) Center for Wave Phenomena, Department of Geophysics, Colorado School of Mines, Golden, Colorado, USA
(2) Department of Geoscience and Engineering, Delft University of Technology, GA Delft, The Netherlands
(3) Seismic Science LLC, Colorado, USA

ABSTRACT

Recent work on autofocusing with the Marchenko equation has shown how the Green's function for a virtual source in the subsurface can be obtained from reflection data. The response to the virtual source is the Green's function from the location of the virtual source to the surface. The Green's function is retrieved using only the reflection response of the medium and an estimate of the first arrival at the surface from the virtual source. Current techniques, however, only include primaries and internal multiples. Therefore, all surface-related multiples must be removed from the reflection response prior to Green's function retrieval. Here, we extend the Marchenko equation to retrieve the Green's function that includes primaries, internal multiples, and free-surface multiples. In other words, we retrieve the Green's function in the presence of a free surface. We use the associated Green's function for imaging the subsurface. The information needed for the retrieval are the reflection response at the surface and an estimate of the first arrival at the surface from the virtual source. The reflection response, in this case, includes the free-surface multiples; this makes it possible to include these multiples in the imaging operator and it obviates the need for surface-related multiple elimination.

1 INTRODUCTION

To focus a wavefield at a point in a medium only requires surface reflection data and an estimate of the first arriving wave at the surface from a point source at the focusing location (Broggini et al., 2012; Broggini and Snieder, 2012; Wapenaar et al., 2013a). Unlike in seismic interferometry (Bakulin and Calvert, 2006), no receivers are required at the desired focusing location, i.e. the virtual source location. Significantly, the detailed medium parameters need not be known to focus the wavefield. However the travel-time of the direct-arrival of the virtual source to the surface is required. To obtain this travel time, one only needs a macro-model of the velocity.

The focusing scheme of Broggini et al. (2012), Broggini and Snieder (2012), and Wapenaar et al. (2013a) is an extension of the algorithm of Rose (2002a,b) who shows an iterative scheme that solves the Marchenko equation for wavefield focusing in one dimension. The focused events in the wavefield for the virtual source consist of primaries and internal multiples (Wapenaar et al., 2013a) but not free-surface multiples. Importantly, Rose (2002a,b) derived the focusing method (autofocusing) for single-sided illumination with sources and receivers on one side of the medium, similar to current geophysical acquisition methods.

We summarize our work in Figure 1. In this paper, any variable with a subscript 0 (e.g R_0) signifies that no free-surface is present. As shown in Figure 1 (solid up-going arrow), for the algorithm of Broggini et al. (2012), one must remove the free-surface multiples from the reflection response of the medium to retrieve the Green's function by autofocusing. The removal of the free-surface multiples can be achieved by Surface Related Multiple Elimination (SRME) (Verschuur et al., 1992).

Wapenaar et al. (2011a) illustrate imaging with the Green's function in 1D and also discuss how to image in multi-dimensions (2D and 3D). Similarly, Behura et al. (2012) introduce an imaging algorithm based on the auto-focusing scheme that images not only primaries but also internal multiples, thereby reducing imaging artifacts. Broggini et al. (2014) extend the work of Behura et al. (2012) by using multidimensional deconvolu-

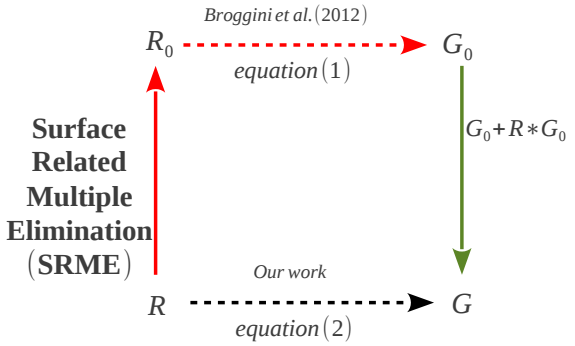

Figure 1. Overview of the methods to focus the wavefield using an iterative approach. R denotes reflected waves recorded at the surface in the presence of a free surface, and R_0 is the reflected waves for a medium without a free surface. G is the Green's function at the surface for a virtual source located at a point in the medium in the presence of a free surface and G_0 is the Green's function in the absence of a free surface. The two dashed arrows indicate separate iterative schemes.

tion (MDD) as the imaging condition in place of conventional cross-correlation or deconvolution, which further reduces the artifacts. In other words, Broggini et al. (2014) retrieve the Green's function from the acquisition surface to any point in the medium. This Green's function is essentially an imaging or downward continuation operator. Since this Green's function includes both primaries and internal multiples, we expect improved subsurface images compared to using primaries alone.

In this paper, we modify the earlier focusing algorithms (Rose, 2002a; Broggini et al., 2012; Wapenaar et al., 2013a) to focus not only primaries and internal multiples but also the free-surface multiples; this is labeled **Our Work** in Figure 1. We achieve such focusing using reflected waves in the presence of a free surface and an estimate of the first arrival from the focus location to the surface. Notably, our proposed auto-focusing scheme obviates the need for SRME (Figure 1).

The free surface is the strongest reflector in the system; therefore, in general, the free-surface multiples are stronger than internal multiples. In addition, free-surface multiples can be used to provide better illumination, higher fold, and better vertical resolution of the subsurface (Schuster et al., 2003; Jiang et al., 2007; Muijs et al., 2007a,b). For these reasons, by retrieving the Green's function which includes primaries and all multiples (including free-surface multiples) and using the imaging condition proposed by Behura et al. (2012), we expect better imaging of the subsurface.

2 THEORY

The theory of focusing the wavefield without a free surface, i.e. retrieving the Green's function G_0, is covered by Rose (2002a), Broggini et al. (2012), and Wapenaar et al. (2013a). As summarized in Figure 1, we have to remove the free-surface multiples from the reflection response R (by SRME) to get R_0 and then compute G_0, the Green's function in the absence of the free surface.

We can retrieve G (the Green's function in the presence of the free surface) from G_0 in the frequency domain with the expression

$$G(\mathbf{x}_\mathbf{i}', \mathbf{x_0}, \omega) = G_0(\mathbf{x}_\mathbf{i}', \mathbf{x_0}, \omega) - \int_{\partial D_0} G_0(\mathbf{x}_\mathbf{i}', \mathbf{x}, \omega) R(\mathbf{x}, \mathbf{x_0}, \omega) d\mathbf{x}, \quad (1)$$

where ∂D_0 is the acquisition surface, $\mathbf{x_0}$ and $\mathbf{x}_\mathbf{i}'$ are spatial positions along ∂D_0 and ∂D_i (arbitrary depth level), and R is the reflection response for a down-going incident wavefield. Equation 1 is shown in Figure 1 by the solid down-going arrow. This method of retrieving G from G_0 follows from Equation 22 of Wapenaar et al. (2004) which relates the transmission operators for media with and without the free surface. In our case, we replace the transmission operators with the corresponding Green's functions, G or G_0, since the Green's function is the total transmitted wavefield from the focusing point to the surface that includes multiples. Note that this approach, $R \rightarrow R_0 \rightarrow G_0 \rightarrow G$, follows the tortuous path shown in Figure 1. We can, however, retrieve the Green's function in the presence of the free surface directly from the measured reflection data $R \rightarrow G$ (Figure 1, black arrow). This avoids the more elaborate path $R \rightarrow R_0 \rightarrow G_0 \rightarrow G$ so that SRME and G_0 are not required.

We generalize the formulation of Wapenaar et al. (2013a) to include free-surface multiples ($R \rightarrow G$); the detailed mathematics of this retrieval is documented in the appendix. The reflections from the free surface are included in the focusing scheme similar to the treatment by Wapenaar et al. (2004) of free-surface multiples.

We define our spatial vector field by its horizontal coordinates and depth coordinates, for instance $\mathbf{x_0} = (\mathbf{x_H}, x_{3,0})$, where $\mathbf{x_H}$ are the horizontal coordinates at a depth $x_{3,0}$. We define a solution for the waves that focus at a point in a medium, called the focusing functions f_1 and f_2. The f_1 function involves waves that focus at $\mathbf{x}_\mathbf{i}'$ at a defined depth level (∂D_i) for incoming and outgoing waves at the acquisition surface (∂D_0) at $\mathbf{x_0}$ (Figure 2). The function f_2 is somewhat the opposite of f_1 as it is a solution for waves that focus just above ∂D_0 at $\mathbf{x_0''}$ for incoming and outgoing waves at ∂D_i (Figure 3). The focusing functions exist in a reference medium that has the same material properties as the actual inhomogeneous medium between ∂D_0 and ∂D_i and that is homogeneous above ∂D_0 and reflection-free below ∂D_i (Slob et al., 2014). Therefore, the boundary conditions on ∂D_0 and ∂D_i in the reference medium, where the focusing function exists, are reflection free. Note that this boundary condition need not be the same as the actual medium. The focusing functions can be separated into

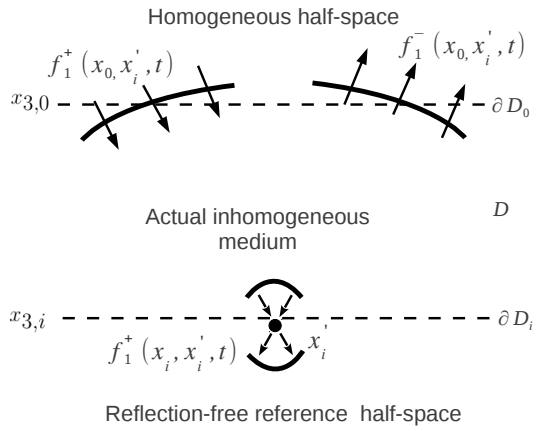

Figure 2. Focusing function f_1 that focuses at $\mathbf{x_i'}$.

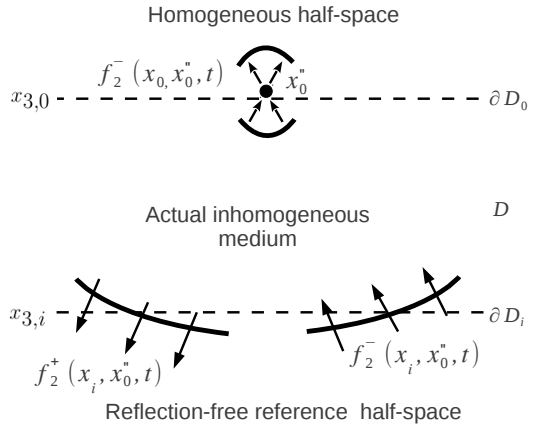

Figure 3. Focusing function f_2 that focuses at $\mathbf{x_0''}$.

up-going and down-going waves; the first focusing function in the frequency domain reads (Wapenaar et al., 2013a)

$$f_1(\mathbf{x}, \mathbf{x_i'}, \omega) = f_1^+(\mathbf{x}, \mathbf{x_i'}, \omega) + f_1^-(\mathbf{x}, \mathbf{x_i'}, \omega), \qquad (2)$$

while the second focusing function reads

$$f_2(\mathbf{x}, \mathbf{x_0''}, \omega) = f_2^+(\mathbf{x}, \mathbf{x_0''}, \omega) + f_2^-(\mathbf{x}, \mathbf{x_0''}, \omega), \qquad (3)$$

In this paper the superscirpt $(+)$ refer to down-going waves and $(-)$ to up-going waves.

The focusing functions are the same regardless of the surface boundary condition of the actual medium as these functions reside only in the reference medium. The focusing function f_2 consists of the direct arriving wave and the coda M following the direct arrival. The coda M consists of the scattered waves that result when the direct arriving wave transmits through the medium to the focus point.

The second focusing function is related to the Green's function G_0 of the actual inhomogeneous medium without a free surface by (Wapenaar et al., 2013a):

$$G_0(\mathbf{x_i'}, \mathbf{x_0''}, \omega) = f_2(\mathbf{x_i'}, \mathbf{x_0''}, \omega)^* + \int_{\partial D_0} f_2(\mathbf{x_i'}, \mathbf{x_0}, \omega) R_0(\mathbf{x_0}, \mathbf{x_0''}, \omega) d\mathbf{x_0}. \qquad (4)$$

As shown in the appendix, the Green's function in the presence of the free surface is given by

$$G(\mathbf{x_i'}, \mathbf{x_0''}, \omega) = f_2(\mathbf{x_i'}, \mathbf{x_0''}, \omega)^* + \int_{\partial D_0} f_2(\mathbf{x_i'}, \mathbf{x_0}, \omega) R(\mathbf{x_0}, \mathbf{x_0''}, \omega) d\mathbf{x_0} + r \int_{\partial D_0} f_2(\mathbf{x_i'}, \mathbf{x_0}, \omega)^* R(\mathbf{x_0}, \mathbf{x_0''}, \omega) d\mathbf{x_0}, \qquad (5)$$

where * represents the complex conjugate, and $r = -1$ is the reflection coefficient of the free surface. The reflection response R is flux-normalized so that the one-way reciprocity equations (Wapenaar and Grimbergen, 1996) hold. Note the up-going Green's function (G^-) in the actual inhomogeneous medium at ∂D_0 is the reflection response R for a downward radiating source at ∂D_0.

Equation 5 differs from equation 4 in two ways. First, the last term on the right hand side of equation 5 accounts for the waves that are reflected off the free surface. Second, equation 5 contains the reflection coefficient R for a medium with a free surface, while expression 4 contains the reflection coefficients R_0 for a medium without a free surface.

Similar to our treatment of the focusing function f_2, we can define another focusing function g_2 such that

$$g_2(\mathbf{x}, \mathbf{x_0''}, \omega) = f_2^+(\mathbf{x}, \mathbf{x_0''}, \omega) - f_2^-(\mathbf{x}, \mathbf{x_0''}, \omega). \qquad (6)$$

Analogously, we can define a difference Green's function $\widetilde{G}$ that is related to g_2 similar to expression 5 by

$$\widetilde{G}(\mathbf{x_i'}, \mathbf{x_0''}, \omega) = g_2(\mathbf{x_i'}, \mathbf{x_0''}, \omega)^* - \int_{\partial D_0} g_2(\mathbf{x_i'}, \mathbf{x_0}, \omega) R(\mathbf{x_0}, \mathbf{x_0''}, \omega) d\mathbf{x_0} + r \int_{\partial D_0} g_2(\mathbf{x_i'}, \mathbf{x_0}, \omega)^* R(\mathbf{x_0}, \mathbf{x_0''}, \omega) d\mathbf{x_0}. \qquad (7)$$

We call $\widetilde{G}$ the difference Green's function since

$$\widetilde{G}(\mathbf{x_i'}, \mathbf{x_0''}, \omega) = G^+(\mathbf{x_i'}, \mathbf{x_0''}, \omega) - G^-(\mathbf{x_i'}, \mathbf{x_0''}, \omega). \qquad (8)$$

To yield the up-going Green's function, we subtract equations 5 and 8:

$$G^-(\mathbf{x_i'}, \mathbf{x_0''}, \omega) = {}^1\!/_2 [G(\mathbf{x_i'}, \mathbf{x_0''}, \omega) - \widetilde{G}(\mathbf{x_i'}, \mathbf{x_0''}, \omega)]. \qquad (9)$$

Similarly, we obtain the down-going Green's function by adding equations 5 and 8:

$$G^{+}(\mathbf{x_i}', \mathbf{x_0}'', \omega) = {}^1\!/_2[G(\mathbf{x_i}', \mathbf{x_0}'', \omega) + \widetilde{G}(\mathbf{x_i}', \mathbf{x_0}'', \omega)]. \quad (10)$$

These up- and down-going (G^{+} and G^{-}) Green's functions at the focal point are used for imaging and include primaries and all multiples. The up- and down-going Green's functions have been used for imaging the subsurface, (Behura et al., 2012; Broggini et al., 2014, 2012; Wapenaar et al., 2011a). However, their Green's function only contains primaries and internal multiples. In this paper, the up- and down-going Green's function also includes free-surface multiples.

The use of up- and down-going wavefield for imaging is not a new principle. Claerbout (1971), Wapenaar et al. (2000) and Amundsen (2001) have shown that one can get the reflection coefficient below an arbitrary depth level once the up- and down-going wavefields are available. The governing equation for imaging with these up- and down-going waves is

$$G^{-}(\mathbf{x_i}', \mathbf{x_0}'', t) = \int_{\partial D_i} d\mathbf{x_i} \int_{-\infty}^{\infty} G^{+}(\mathbf{x_i}', \mathbf{x_0}'', t - t') R_0^{\cup}(\mathbf{x_i}, \mathbf{x_i}', t') dt', \quad (11)$$

where ∂D_i is an arbitrary depth level, $R_0^{\cup}$ is the reflection response below ∂D_i. In addition, $R_0^{\cup}$ at ∂D_i is reflection-free above this depth level. We can think of $R_0^{\cup}$ as the reflection response from a truncated medium; where the truncated medium is the same as the true medium below ∂D_i and reflection free above. Equation 11 states that we can recover G^{-} from the convolution of G^{+} with $R_0^{\cup}$ and integrate along all source positions x' of $R_0^{\cup}$.

We solve for $R_0^{\cup}$ by multidimensional deconvolution (Wapenaar et al., 2008, 2011b) as the time integral is a convolution. The subsurface image is given by taking the zero lag of $R_0^{\cup}$, i.e. $t = 0$ at each depth level in the model, (for each ∂D_i), this is called the multidimensional imaging condition. Alternatively, once we obtain $R_0^{\cup}$ at an arbitrary ∂D_i we can also apply a standard imaging procedure, for instance, downward continuation, to image below ∂D_i. This is because $R_0^{\cup}$ is the reflection response of the truncated medium below ∂D_i for sources and receivers at ∂D_i.

3 NUMERICAL EXAMPLES

We consider a 1D model that has a high impedance layer generic to salt models as shown in Figure 4. A Receiver at the surface records the reflected waves. To retrieve the Green's function in 1D, one needs the travel time of the first arriving wave from the virtual source to the surface. In 2D or 3D media, a smooth version of the slowness (1/velocity) can be used to get an estimate of the direct arriving wave from the virtual source to the surface. The direct arriving wave can be obtained using finite-difference modeling of the waveforms.

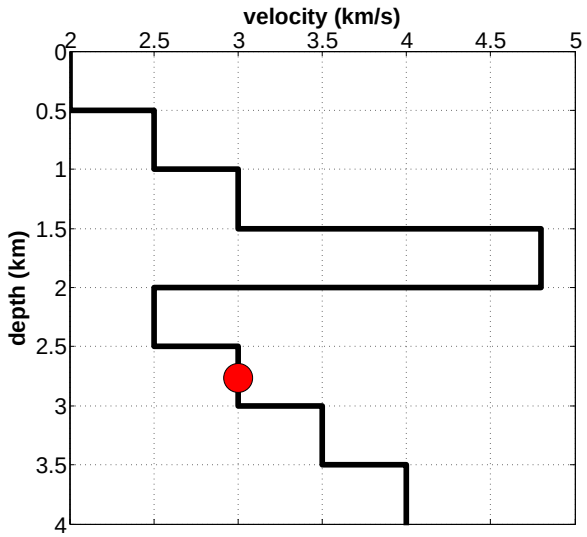

Figure 4. Velocity model with high impedance layer at 1.5 km; the dot is the position of the virtual source.

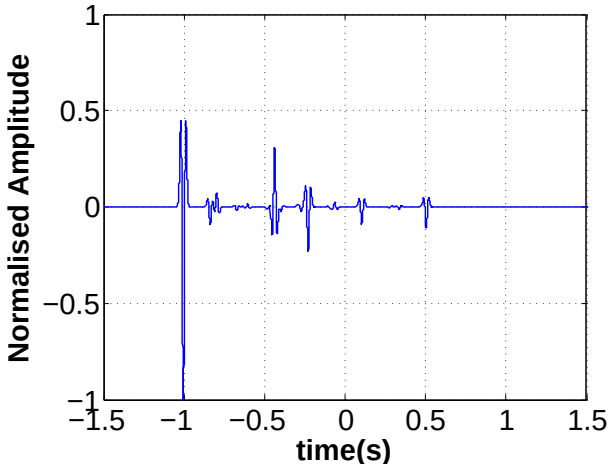

Figure 5. Focusing function f_2 at depth 2.75 km.

We obtain the focusing function f_2, Figure 5, by setting the left-hand side of equation 5 to zero and evaluating this expression for a time earlier than the first arriving wave. (Details are given in equations A8 and A7 of the Appendix). The focusing function is substituted in equation 5 to retrieve the Green's function located at 2.75 km to the surface, Figure 6. This Green's function G, arbitrarily scaled to its maximum amplitude (Figure 6), is the response at the surface ∂D_0 to the virtual source (located at 2.75 km [dot in Figure 4]).

We also model the Green's function using finite dif-

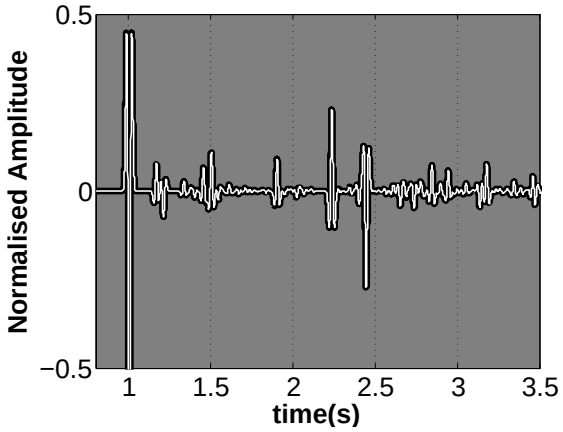

Figure 6. Retrieved Green's function (normalized by maximum amplitude), G, from a depth of 2.75 km to the surface (white). The model Green's function is displayed (in black) in the background.

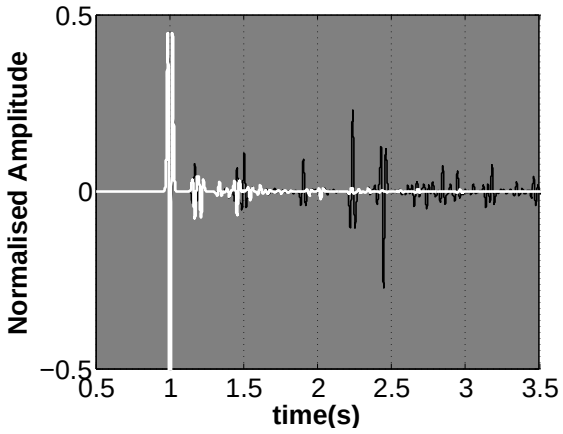

Figure 7. Impact of the free surface. White line: the Green's function in a medium without a free surface G_0, and black line is the difference between G and G_0, therefore the blue line shows events that are caused by the presence of the free surface.

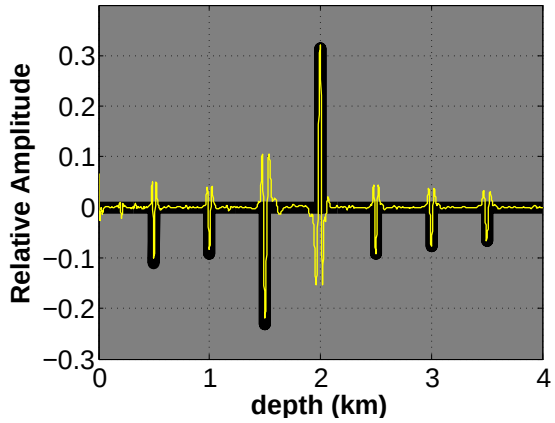

Figure 8. Autofocusing imaging of Figure 4 in yellow, with the true reflectivity (in black) in the background.

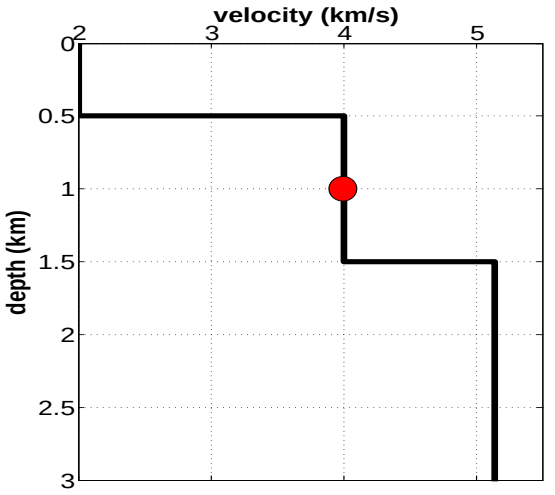

Figure 9. Simple velocity model where the dot indicates the position of one virtual source at depth 1000 m.

ferences to ensure that the Green's function retrieved from our autofocusing algorithm is accurate, and superimposed this result on Figure 6. The vertical scale of Figure 6 is enlarged to better illustrate the model and retrieved Green's function. For this reason, the first arrival at time 1.0 s is clipped. The difference between the modeled and the retrieved Green's function is negligible relative to the average amplitude of the Green's function, as seen in Figure 6, and can be attributed to numerical errors. The arrivals caused by the free surface are shown in Figure 7 compared to the arrivals caused by no free surface. The corresponding autofocus image of the model in Figure 4 illustrates the correct location of the reflectors as well as the correct scaled reflection coefficient shown in Figure 8. In 1D, the autofocus image is the deconvolution of the up- and down-going Green's function at each image point for $t = 0$. There are some anomalous amplitudes in the autofocus image (especially around 200 m) but they are small compared to the actual reflectors' amplitude.

The next example is taken from Weglein and Dragoset (2007), where the second primary event cancels with the free surface multiple. I demonstrate with this numerical example the retrieval of the Green's function (as well as its associated up- and down-going Green's function) at depth 1000m for the model shown in Figure 9. The associated reflected waves at the acquisition level, shown in Figure 10, are recorded 5m below the free surface. Figure 11 illustrates some of the events that are present in the reflection response. As is shown

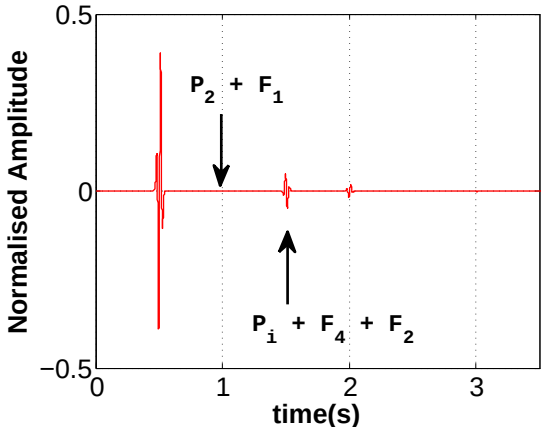

Figure 10. Reflection response with the direct waves removed (The events are scaled by the direct wave magnitude), labels are referenced to Figure 11.

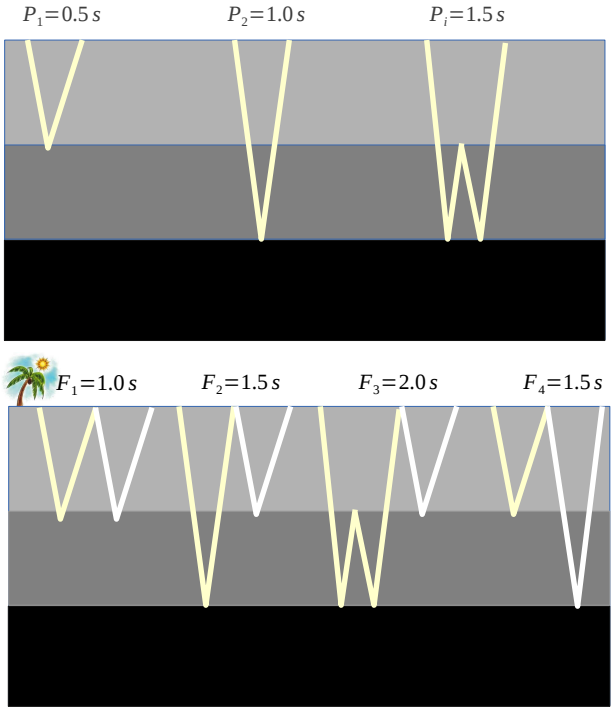

Figure 11. Sketch of some events that occur in the velocity model in Figure 9.

in Figures 10 and 11, the second primary event P_2 is canceled by the free-surface multiple F_1 at 1.0 s, and the other events (internal multiples and free surface multiples) interfere destructively with each other at later times.

One needs to remove the multiples before implementing standard imaging; however, using SRME with adaptive subtraction for this removal will be problematic as the primary and the free surface multiples completely cancels each other at 1.0 s, and even at later travel times the multiples interfere destructively with the primaries. Hence it will be difficult to image the second reflector by SRME followed by standard imaging.

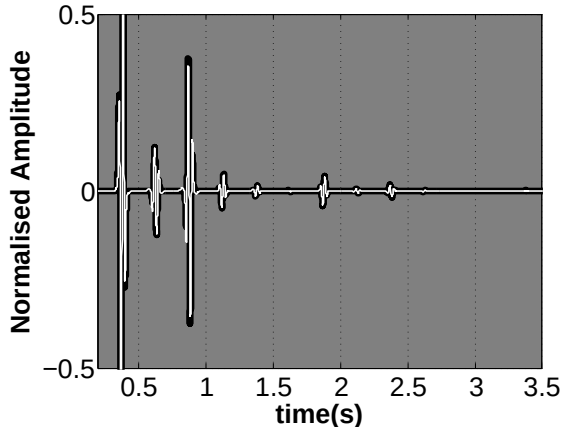

Figure 12. Green's function with virtual source at depth 1000 m and recording at the surface. The black thicker line is the modeled Green's function, superimposed on it is the retrieved Green's function from autofocusing. The plot limits are chosen between 0.5 to -0.5 normalized amplitude to visualize the smaller amplitude events better.

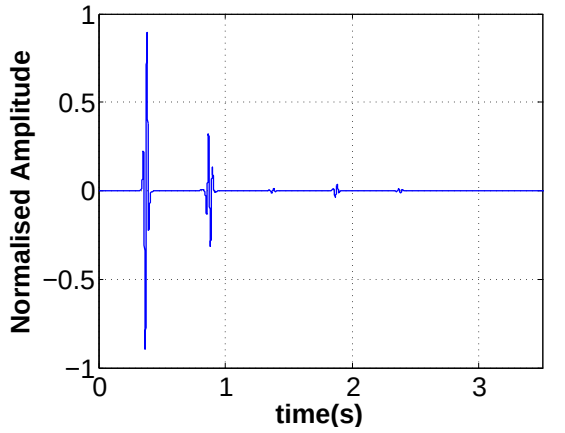

Figure 13. Up-going Green's function with virtual source at depth 1000 m and recording at the surface.

The Green's function for a source at depth 1000m is shown in Figure 12. The corresponding up- and down-going Green's function at depth 1000 m is illustrated in Figures 13 and 14, respectively. The computed travel times for this simple model of the up- and down-going Green's function Figure 15 corresponds with the events in the retrieved up- and down-going Green's functions; hence verifying our decomposition of the Green's function into its associated up- and down-going wavefields.

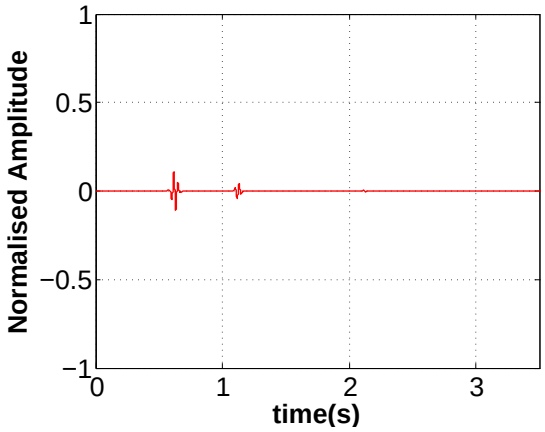

Figure 14. Down-going Green's function with virtual source at depth 1000 m and recording at the surface.

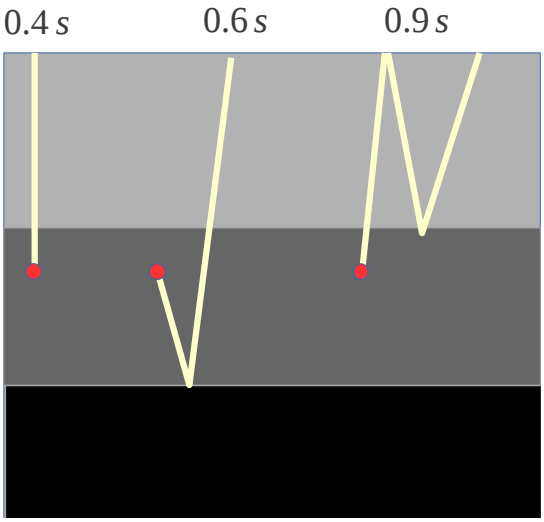

Figure 15. Sketch of some events that are present in the Green's function from the virtual source (red dot) at 1000m and recorded at the surface.

Figure 12 has an event at 0.6 seconds, which is the reflection of the virtual source from the second layer recorded at the surface. Therefore, the Green's function algorithm correctly detects the missing reflector in the recorded waves. Consequently, applying the deconvolution imaging condition, equation 11, to the up- and down-going Green's function at every point in the velocity model yields the correct positioning of the reflectors, see Figure 16, as well as the correct scaled reflection coefficient.

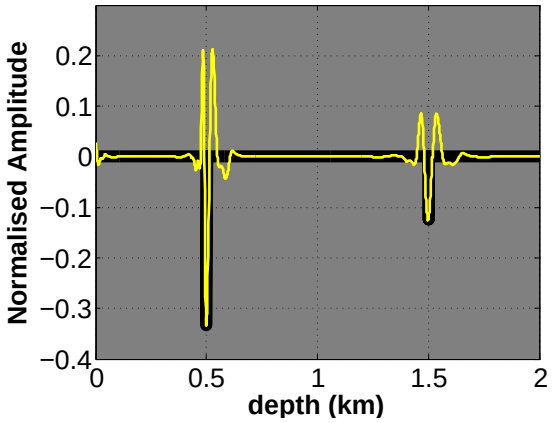

Figure 16. Image of the velocity model after autofocusing imaging with the reflectivity overlain (in black).

4 DISCUSSION/CONCLUSION

The advantage of our autofocusing scheme is that we include the free-surface multiples in our Green's function, hence we don't need to remove the free-surface multiples in our reflection response. For our 1D numerical examples, we can isolate the events that are caused by the presence of the free surface (black line in Figure 7) by computing the difference of G and G_0. These arrivals that are caused by the free surface (black line in Figure 7) have higher amplitude and greater waveform complexity compared to the events for the response without a free surface G_0 (white line in 7). This supports our conclusion that using the additional events and energy that free-surface reflections provide can benefit imaging of the subsurface, i.e. imaging using G rather than with G_0.

In our autofocusing scheme we require that the wavelet be removed from the reflection response (which can be done by deconvolution). In addition, we assume that the reflection response is due to a down-going source. However in the marine case the source is generally placed a few meters below the surface, therefore there is not only a down-going component of the source, but also an up-going component. In such situations, we consider the source wavelet to also include the up-going component of the source. Consequently, the wavelet with which we deconvolve the reflection response at the surface is no longer a monopole source but a dipole source.

In summary, we extended the retrieval of the Green's function to include the presence of a free surface. This function includes primaries, internal multiples, and now free-surface multiples. Significantly, our proposed method does not require any surface-related multiple removal of the reflection response. In addition,

we need an estimate of the first arrival at the surface from the virtual source in the subsurface. To obtain the first arrival, we only need a macro model of the velocity, but the small scale details of the velocity and density need not be known.

5 ACKNOWLEDGMENTS

This work was funded by the sponsor companies of the Consortium Project on Seismic Inverse Methods for Complex Structures. We are grateful to Diane Witters for her help in preparing this manuscript.

APPENDIX A: GREEN'S FUNCTION RETRIEVAL IN THE PRESENCE OF THE FREE SURFACE

We discuss our adaptation of the method of Wapenaar et al. (2013b) to account for the free-surface reflections. The focusing functions are the wavefields that focus, in both time and space, at a point in the medium (Figure 2 and 3). These focusing functions exist in the reference medium, which is homogeneous above the depth level ∂D_0 and reflection-free below ∂D_i.

The reciprocity theorems for one-way (up-going and down-going) wavefields are derived by Wapenaar and Grimbergen (1996). We use the convolution-type and correlation-type reciprocity theorems given in Wapenaar and Grimbergen (1996) to find relationships between our up- and down-going wavefields. As discussed by Wapenaar et al. (2013a), we obtain a relationship for the focusing functions (f_1 and f_2) by using their respective up- and down-going waves at each depth level (∂D_0 and ∂D_i) with the convolution reciprocity theorem

$$f_1^+(\mathbf{x_0}^{''}, \mathbf{x_i}^{'}, \omega) = f_2^-(\mathbf{x_i}^{'}, \mathbf{x_0}^{''}, \omega) \tag{A1}$$

and cross-correlation reciprocity theorem

$$-f_1^-(\mathbf{x_0}^{''}, \mathbf{x_i}^{'}, \omega)^* = f_2^+(\mathbf{x_i}^{'}, \mathbf{x_0}^{''}, \omega). \tag{A2}$$

Our actual inhomogeneous model with a free surface above ∂D_0 is shown in Figure A1. As opposed to the model in Wapenaar et al. (2013a) which does not have a free surface, we consider the reflections from the free surface for a down-going source similar to the work of Wapenaar et al. (2004). In Figure A1, we describe the wavefield in its up- and down-going components. The downward propagating component of the wavefield (Green's function) at ∂D_0 is $G^+(\mathbf{x_0}, \mathbf{x_0''}, \omega) = \delta(\mathbf{x_H} - \mathbf{x_H}^{''}) + rR(\mathbf{x_0}, \mathbf{x_0}^{''}, \omega)$, which includes (in the right hand side) the downward-going impulsive source and the reflection from the free surface. The down-going source $\delta(\mathbf{x_H} - \mathbf{x_H}^{''})$ is a 2-dimensional Dirac delta where $\mathbf{x_H}^{''}$ is the lateral position of the focal point.

Note G^+ is the component of the Green's function that is propagating downwards at $\mathbf{x_0}$ for a downward radiating source at $\mathbf{x_0}^{''}$. In the case without the free surface, there are no reflections from the free surface, hence $G_0^+(\mathbf{x_0}, \mathbf{x_0''}, \omega) = \delta(\mathbf{x_H} - \mathbf{x_H}^{''})$ because $r = 0$. The upward-going propagating part of the Green's function G^- above ∂D_0 is the reflection response $R(\mathbf{x_0}, \mathbf{x_0}^{''}, \omega)$. We consider the up- and down-going components of the Green's function just below ∂D_i. The down-going component is $G^+(\mathbf{x_i}, \mathbf{x_0''}, \omega)$ while the up-going component is $G^-(\mathbf{x_i}, \mathbf{x_0''}, \omega)$ (G^+ and G^- respectively, Figure A1). We use the convolution and correlation reciprocity theorems to find relationships for the one-way wavefields of f_1 shown in Figure 2 and the one-way wavefields of the Green's function in the actual medium shown in Figure A1:

$$G^-(\mathbf{x_i}^{'}, \mathbf{x''_0}, \omega) = \int_{\partial D_0} [f_1^+(\mathbf{x_0}, \mathbf{x_i}^{'}, \omega)R(\mathbf{x_0}, \mathbf{x_0}^{''}, \omega) - rf_1^-(\mathbf{x_0}, \mathbf{x_i}^{'}, \omega)R(\mathbf{x_0}, \mathbf{x_0}^{''}, \omega)]d\mathbf{x} - f_1^-(\mathbf{x_0}^{''}, \mathbf{x_i}^{'}, \omega), \tag{A3}$$

and

$$G^+(\mathbf{x_i}^{'}, \mathbf{x_0''}, \omega) = -\int_{\partial D_0} [f_1^-(\mathbf{x_0}, \mathbf{x_i}^{'}, \omega)^* R(\mathbf{x_0}, \mathbf{x_0}^{''}, \omega) - rf_1^+(\mathbf{x_0}, \mathbf{x_i}^{'}, \omega)^* R(\mathbf{x_0}, \mathbf{x_0}^{''}, \omega)]d\mathbf{x} + f_1^+(\mathbf{x''_0}, \mathbf{x_i}^{'}, \omega)^*. \tag{A4}$$

Equations A3 and A4 are similar to the relation for the up- and down-going Green's function in Wapenaar et al. (2013a), however equations A3 and A4 also considers the reflected waves from the free surface. These free-surface reflections are the expressions in equations A3 and A4 that are multiplied by r. The two-way Green's function is obtained by adding equations A3 and A4 as well as using equations 2, 3, A1, and A2:

$$G(\mathbf{x_i}^{'}, \mathbf{x_0''}, \omega) = f_2(\mathbf{x_i}^{'}, \mathbf{x_0}^{''}, \omega)^* + \int_{\partial D_0} f_2(\mathbf{x_i}^{'}, \mathbf{x_0}, \omega)R(\mathbf{x_0}, \mathbf{x_0}^{''}, \omega)d\mathbf{x_0} + r\int_{\partial D_0} f_2(\mathbf{x_i}^{'}, \mathbf{x_0}, \omega)^* R(\mathbf{x_0}, \mathbf{x_0}^{''}, \omega)d\mathbf{x_0}. \tag{A5}$$

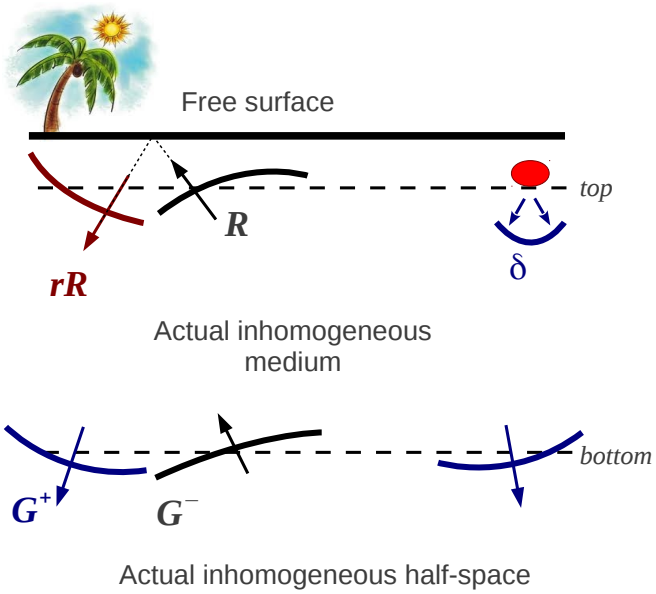

Figure A1. Green's functions in the actual inhomogeneous medium in the presence of a free surface.

We consider equation A5, in time, for the interval $t < t_d(\mathbf{x_i}^{'}, \mathbf{x_0}^{''})$, where t_d is the travel time for the first arrival of G. No waves arrive before $t_d(\mathbf{x_i}^{'}, \mathbf{x_0}^{''})$ since t_d is the time for the first arriving event. Therefore, $G(\mathbf{x_i}^{'}, \mathbf{x_0}^{''}, \omega)$ vanishes for $t < t_d(\mathbf{x_i}^{'}, \mathbf{x_0}^{''})$ and as a result

$$0 = f_2(\mathbf{x_i}^{'}, \mathbf{x_0}^{''}, -t) + \int_{\partial D_0} d\mathbf{x_0} \int_{-\infty}^{t} f_2(\mathbf{x_i}^{'}, \mathbf{x_0}, t^{'}) R(\mathbf{x_0}, \mathbf{x_0}^{''}, t - t^{'}) dt^{'} + r \int_{\partial D_0} d\mathbf{x_0} \int_{-t}^{\infty} f_2(\mathbf{x_i}^{'}, \mathbf{x_0}, t^{'}) R(\mathbf{x_0}, \mathbf{x_0}^{''}, t + t^{'}) dt^{'}. \tag{A6}$$

We use the same ansatz for f_2 as Wapenaar et al. (2013a) because we are using the same reference medium, i.e. the model where the focusing functions exist. The ansatz is given by

$$f_2(\mathbf{x_i}, \mathbf{x_0}^{''}, t) = [T_d(\mathbf{x_i}, \mathbf{x_0}^{''}, t)]^{inv} + M(\mathbf{x_i}, \mathbf{x_0}^{''}, t), \tag{A7}$$

where $[T_d(\mathbf{x_i}, \mathbf{x_0}^{''}, t)]^{inv}$, defined as the inverse of the direct arrival of the transmission response, is the first arriving event of $f_2(\mathbf{x_i}, \mathbf{x_0}^{''}, t)$ and $M(\mathbf{x_i}, \mathbf{x_0}^{''}, t)$ is the scattering coda of f_2 following the first arrival as shown by Wapenaar et al. (2013a). The substitution of expression A7 in equation A6 yields

$$\begin{aligned} 0 = M(\mathbf{x_i}^{'}, \mathbf{x_0}^{''}, -t) + & \int_{\partial D_0} d\mathbf{x_0} \int_{-\infty}^{-t_d^{\epsilon}} [T_d(\mathbf{x_i}^{'}, \mathbf{x_0}, t')]^{inv} R(\mathbf{x_0}, \mathbf{x_0}^{''}, t - t^{'}) dt^{'} \\ + & \int_{\partial D_0} d\mathbf{x_0} \int_{-t_d^{\epsilon}(\mathbf{x_i}^{'}, \mathbf{x_0})}^{t} M(\mathbf{x_i}^{'}, \mathbf{x_0}, t') R(\mathbf{x_0}, \mathbf{x_0}^{''}, t - t^{'}) dt^{'} \\ + r & \int_{\partial D_0} d\mathbf{x_0} \int_{-t_d^{\epsilon}(\mathbf{x_i}^{'}, \mathbf{x_0})}^{\infty} M(\mathbf{x_i}^{'}, \mathbf{x_0}, t') R(\mathbf{x_0}, \mathbf{x_0}^{''}, t + t^{'}) dt^{'} \end{aligned} \tag{A8}$$

for $t < t_d(\mathbf{x_i}^{'}, \mathbf{x_0}^{''})$ with $t_d^{\epsilon}(\mathbf{x_i}^{'}, \mathbf{x_0}^{''}) = t_d(\mathbf{x_i}^{'}, \mathbf{x_0}^{''}) - \epsilon$ where ϵ is a small positive constant to include the direct arrival in the integral. Equation A8 is a Fredholm integral of the second kind and can be solved iteratively as follows:

$$\begin{aligned} M_k(\mathbf{x_i}^{'}, \mathbf{x_0}^{''}, -t) = M_0(\mathbf{x_i}^{'}, \mathbf{x_0}^{''}, -t) - & \int_{\partial D_0} d\mathbf{x_0} \int_{-t_d(\mathbf{x_i}^{'}, \mathbf{x_0})}^{\infty} M_{k-1}(\mathbf{x_i}^{'}, \mathbf{x_0}, t') R(\mathbf{x_0}, \mathbf{x_0}^{''}, t - t^{'}) dt^{'} \\ - r & \int_{\partial D_0} d\mathbf{x_0} \int_{-t_d(\mathbf{x_i}^{'}, \mathbf{x_0})}^{\infty} M_{k-1}(\mathbf{x_i}^{'}, \mathbf{x_0}, t') R(\mathbf{x_0}, \mathbf{x_0}^{''}, t + t^{'}) dt^{'}, \end{aligned} \tag{A9}$$

where

$$M_0(\mathbf{x_i}^{'}, \mathbf{x_0}^{''}, -t) = - \int_{\partial D_0} d\mathbf{x_0} \int_{-\infty}^{\infty} [T_d(\mathbf{x_i}^{'}, \mathbf{x_0}, t')]^{inv} R(\mathbf{x_0}, \mathbf{x_0}^{''}, t - t^{'}) dt^{'} \tag{A10}$$

for $t < t_d(\mathbf{x_i}', \mathbf{x_0}'')$. In contrast to the algorithm of Wapenaar et al. (2013a), we use R instead of R_0 and we also include the reflection from the free surface (last term in equation A10). We substitute the coda M into equation A7 to yield the focusing function f_2. The f_2 solution is then used in equation A5 to obtain the two-way Green's function (equation 5).

REFERENCES

Amundsen, L., 2001, Elimination of free-surface related multiples without need of the source wavelet: Geophysics, **66**, 327–341.

Bakulin, A., and R. Calvert, 2006, The virtual source method: Theory and case study: Geophysics, **71**, SI139–SI150.

Behura, J., K. Wapenaar, and R. Snieder, 2012, Newton-Marchenko-Rose imaging, *in* SEG Technical Program Expanded Abstracts 2012: Society of Exploration Geophysicists, 1–6.

Broggini, F., and R. Snieder, 2012, Connection of scattering principles: a visual and mathematical tour: European Journal of Physics, **33**, 593–613.

Broggini, F., R. Snieder, and K. Wapenaar, 2012, Focusing the wavefield inside an unknown 1d medium: Beyond seismic interferometry: Geophysics, **77**, A25–A28.

Broggini, F., R. Snieder, K. Wapenaar, and J. Behura, 2014, Wave field autofocusing and imaging with multidimensional deconvolution: numerical examples for reflection data with internal multiples: submitted to Geophysics.

Claerbout, J., 1971, Toward a unified theory of reflector mapping: Geophysics, **36**, 467–481.

Jiang, Z., J. Sheng, J. Yu, G. Schuster, and B. Hornby, 2007, Migration methods for imaging different-order multiples: Geophysical Prospecting, **55**, 1–19.

Muijs, R., A. Robertsson, J. O., and K. Holliger, 2007a, Prestack depth migration of primary and surface-related multiple reflections: Part I: Imaging: Geophysics, **72**, S59–S69.

———, 2007b, Prestack depth migration of primary and surface-related multiple reflections: Part II: Identification and removal of residual multiples: Geophysics, **72**, S71–S76.

Rose, J., 2002a, 'Single-sided'autofocusing of sound in layered materials: Inverse problems, **18**, 1923–1934.

———, 2002b, Time reversal, focusing and exact inverse scattering: Imaging of complex media with acoustic and seismic waves, 97–106.

Schuster, G. T., Z. Jiang, and J. Yu, 2003, Imaging the most bounce out of multiples: Presented at the 65th Annual Conference, EAGE Expanded Abstracts: session on Multiple Elimination.

Slob, E., K. Wapenaar, F. Broggini, and R. Snieder, 2014, Seismic reflector imaging using internal multiples with marchenko-type equations: Geophysics, **79**, S63–S76.

Verschuur, D., A. Berkhout, and C. Wapenaar, 1992, Adaptive surface-related multiple elimination: Geophysics, **57**, 1166–1177.

Wapenaar, C., and J. Grimbergen, 1996, Reciprocity theorems for one-way wavefields: Geophysical Journal International, **127**, 169–177.

Wapenaar, K., F. Broggini, E. Slob, and R. Snieder, 2013a, Three-dimensional single-sided marchenko inverse scattering, data-driven focusing, green's function retrieval, and their mutual relations: Phys. Rev. Lett., **110**, no. 8, 084301.

Wapenaar, K., F. Broggini, R. Snieder, et al., 2011a, A proposal for model-independent 3D wave field reconstruction from reflection data: 2011 SEG Annual Meeting, Society of Exploration Geophysicists, 3788–3792.

Wapenaar, K., J. Fokkema, M. Dillen, P. Scherpenhuijsen, et al., 2000, One-way acoustic reciprocity and its applications in multiple elimination and time-lapse seismics: Presented at the 2000 SEG Annual Meeting, Society of Exploration Geophysicists.

Wapenaar, K., E. Slob, and R. Snieder, 2008, Seismic and electromagnetic controlled-source interferometry in dissipative media: Geophysical Prospecting, **56**, 419–434.

Wapenaar, K., E. Slob, J. van der Neut, J. Thorbecke, F. Broggini, and R. Snieder, 2013b, Three-dimensional Marchenko equation for Greens function retrieval beyond seismic interferometry: Presented at the 83rd Annual International meeting of the SEG.

Wapenaar, K., J. Thorbecke, and D. Draganov, 2004, Relations between reflection and transmission responses of three-dimensional inhomogeneous media: Geophysical Journal International, **156**, 179–194.

Wapenaar, K., J. Van Der Neut, E. Ruigrok, D. Draganov, J. Hunziker, E. Slob, J. Thorbecke, and R. Snieder, 2011b, Seismic interferometry by crosscorrelation and by multidimensional deconvolution: a systematic comparison: Geophysical Journal International, **185**, 1335–1364.

Weglein, A., and W. Dragoset, 2007, Multiple attenuation: Society of Exploration Geophysicists, **23**, 482.